Journal of Materials Chemistry C

COMMUNICATION

View Article Online
View Journal | View Issue

High efficiency P3HT:PCBM solar cells with an inserted PCBM layer†

Cite this: J. Mater. Chem. C, 2014, 2, 4383

Received 2nd January 2014
Accepted 10th March 2014

DOI: 10.1039/c4tc00003j

www.rsc.org/MaterialsC

Dan Chi,[ab] Shengchun Qu,[a] Zhanguo Wang*[a] and Jizheng Wang*[b]

By inserting a PCBM (phenyl-C61-butyric acid methyl ester) layer between a P3HT (poly(3-hexylthiophene)):PCBM blend and a Ca/Al cathode, the performance of P3HT:PCBM bulk-heterojunction polymer solar cells is greatly improved. The maximum power conversion efficiency reached 4.24%, which is much higher than that of the traditional standard P3HT:PCBM based device (3.57%). By exploring various experimental techniques including absorption spectroscopy, X-ray photoelectron spectroscopy and impedance spectroscopy, we have found that the enhancement of the device performance can mainly be attributed to two reasons: (1) the inserted-PCBM layer can enhance the overall light absorption of the whole device and hence improve the photocurrent. (2) The inserted-PCBM layer can increase the amount of PCBM at the interface between the active layer and the cathode electrode, and hence suppress carrier recombination and facilitate electron extraction.

Bulk-heterojunction based organic photovoltaic (OPV) cells consisting of polymer donors and fullerene acceptors exhibit great potential due to their low cost, light weight and ease of fabrication.[1–4] In recent years the power conversion efficiency (PCE) of OPV cells has been substantially improved and it has already reached the milestone value of 10%.[5–10] Although great progress has been achieved in the field of OPV cells, their performances are still far behind that of inorganic or organic–inorganic hybrid solar cells.[11–15] Poly(3-hexylthiophene) (P3HT) and phenyl-C61-butyric acid methyl ester (PCBM) are commonly used donor and acceptor materials, respectively, and their blend can achieve a high PCE of about 3.5 to 5.0%.[16–20] They remain the most general and popular material combination for many fundamental and conceptual studies.

It is known that the performance of the active blend layer composed of P3HT and PCBM is very sensitive to even very small variations during film formation processes, such as the temperature in a nitrogen glove box where the spin-coating and solvent annealing are usually carried out, the weight ratio of P3HT to PCBM in the blend and the post-treatments for the spin-coated blend film.[21,22] All of these factors can play critical roles in affecting the morphology of the bulk-heterojunction film. Consequently, the PCE of the P3HT:PCBM blend device can vary widely (usually in a range of 2.0% to 4.0% depending on how well the experimental conditions are controlled). One interesting observation is that the surface of the formed P3HT:PCBM blend film is P3HT-rich instead of PCBM-rich, which is not beneficial for electron extraction because the cathode electrode is usually deposited on this surface.[16] Thus, a PCBM-rich surface is needed. In the previous reports, Tremolet de Villers and his coworkers improved the performance of their P3HT:PCBM blend device and avoided S-shaped current density–voltage (J–V) curves by spin-coating 20 nm PCBM on the surface of the P3HT:PCBM active layer.[21] Liu and Lee increased the PCE of their P3HT:PCBM device by depositing a PCBM layer on the surface of their P3HT:PCBM blend layer.[22] However, these works did not improve the PCE of the P3HT:PCBM solar cell up to 4%.

In light of these developments, here various thicknesses of the PCBM layer in the range of 0 to 20 nm are inserted between the P3HT:PCBM blend layer and calcium/aluminium (Ca/Al) cathode electrode, and the corresponding device performances are investigated. The device with a 15 nm inserted PCBM layer achieves a PCE of 4.24%, much higher than that of the original device without the inserted-PCBM layer (3.57%). The enhancement is mainly due to an increase of 9.7% of the J_{SC} (short circuit current density) and 10.7% of the FF (fill factor). Detailed studies show that the inserted PCBM layer forms PCBM-abundant regions in the interface between the active layer and the cathode, which reduces the carrier recombination at the

[a]Key Laboratory of Semiconductor Materials Science, Institute of Semiconductors, Chinese Academy of Sciences, Beijing, 100083, People's Republic of China. E-mail: zgwang@semi.ac.cn

[b]Beijing National Laboratory for Molecular Sciences, CAS Key Laboratory of Organic Solids, Institute of Chemistry, Chinese Academy of Sciences, Beijing 100190, People's Republic of China. E-mail: jizheng@iccas.ac.cn

† Electronic supplementary information (ESI) available. See DOI: 10.1039/c4tc00003j

interface. Moreover, it also slightly improves the overall light absorption. As a result, J_{SC} and FF are enhanced.

The structure of the device with the inserted PCBM layer is shown in Fig. 1(a). Fig. 1(b) presents the curves of the J_{SC}, FF, and PCE *vs.* the inserted-PCBM layer thickness (0 to 20 nm). It is seen that the optimal thickness for the inserted-PCBM layer is 15 nm. It is worth noting that V_{OC} (open circuit voltage) remains nearly unchanged with varying inserted-PCBM layer thickness, and the corresponding curves are not given here. The parameters of these devices and the *J–V* curves are displayed in Table 1 and Fig. 2(a), respectively. It is seen that the devices with an inserted-PCBM layer all perform better than the device without the inserted-PCBM layer, with higher FF and J_{SC} values (V_{OC} remains almost unchanged). The device with 15 nm inserted-PCBM works the best: $V_{OC} = 0.615$ V, $J_{SC} = 10.06$ mA cm^{-2}, FF = 68.5%, PCE = 4.24%, R_s (series resistance) = 6.60 Ω cm^2 and R_{sh} (shunt resistance) = 2.28 kΩ cm^2, which are all much better results than those of the device without the inserted-PCBM layer ($V_{OC} = 0.616$ V, $J_{SC} = 9.17$ mA cm^{-2}, FF = 61.9%, PCE = 3.57%, R_s = 11.58 Ω cm^2 and R_{sh} = 1.10 kΩ cm^2). The enhanced properties are mainly due to the enhancement of about 9.70% in the J_{SC} and 10.7% in the FF. As we know, the FF is an important parameter that determines the PCE of an OPV cell, and it can be affected by many factors, such as the shunt resistance R_{sh} and the series resistance R_s.[23] From the equivalent circuit of a solar cell device and a very fundamental point of view, larger R_{sh} and lower R_s are beneficial to obtain a higher FF.[24–26] This can also be clearly seen in our devices (Table 1). As the inserted-PCBM layer increases from 0 to 15 nm the R_{sh} keeps increasing and so does the FF, then the R_{sh} and FF start to decrease with a further increase in the inserted-PCBM layer thickness to 20 nm. An opposite trend and its relation with FF are observed for R_s when increasing the inserted-PCBM layer thickness.

The external quantum efficiency (EQE) spectra of the device without the inserted-PCBM layer and the device with the 15 nm inserted-PCBM layer are shown in Fig. 2(b). Apparently the EQE value of the device with the 15 nm inserted-PCBM layer is higher than that of the device without the inserted-PCBM layer (which is consistent with the information in Table 1: the device with inserted PCBM has higher J_{SC}). Fig. 2(c) shows the influence of the PCBM layer on light absorption. By comparing the absorption spectra of the devices with different thicknesses of the inserted-PCBM layer, it can be clearly seen that the light absorption increases with the increasing thickness of the inserted-PCBM layer. These results indicate that the inserted PCBM layer can enhance the overall light absorption of the device.

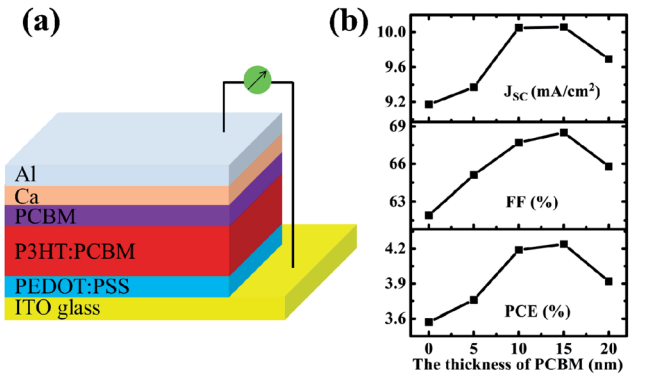

Fig. 1 (a) The schematic structure of the solar cells. (b) J_{SC}, FF and PCE *vs.* inserted PCBM layer thickness (from 0 nm to 20 nm).

To investigate the influence of the inserted-PCBM layer on exciton generation and dissociation, the maximum exciton generation rate (G_{max}) and exciton dissociation probability ($P(E,T)$) of the device with the best performance (with the 15 nm inserted-PCBM layer) and the device without the inserted-PCBM layer were calculated based on the theory reported.[27,28] Fig. 2(d) reveals the dependence of the photocurrent density (J_{ph}) on the effective voltage (V_{eff}) of these two OPV cells. Here, J_{ph} is described using $J_{ph} = J_L - J_D$, where J_L and J_D are the current densities under illumination and in the dark, respectively. V_{eff} is described using $V_{eff} = V_0 - V_a$, where V_0 is the voltage when J_{ph} equals zero and V_a is the applied voltage.[10,29] It can be observed that the J_{ph} increases linearly at a low value of V_{eff} and is saturated at a high value of V_{eff}. Supposing that all of the photogenerated excitons are dissociated and then collected by the electrodes at a high effective voltage, the saturation current density (J_{sat}) will be independent of the bias and temperature but will be limited by the number of the absorbed photons. The value of G_{max} can be obtained by $J_{sat} = qG_{max}L$, where q is the electronic charge and L is the thickness of the active layer (200 nm and 215 nm for the device without the inserted-PCBM layer and the device with the 15 nm inserted-PCBM layer, respectively).[10,29] The values of the G_{max} for the device without the inserted-PCBM layer and the device with the 15 nm inserted-PCBM layer are 2.97×10^{27} m^{-3} s^{-1} ($J_{sat} = 9.51$ mA cm^{-2}) and 3.03×10^{27} m^{-3} s^{-1} ($J_{sat} = 10.41$ mA cm^{-2}), respectively. It is noticeable that the inserted-PCBM layer improves the G_{max}. Since the G_{max} value implies the maximum amount of absorbed photons, an enhanced G_{max} indicates that the PCBM layer improves the light absorption. Another important parameter, *i.e.* the exciton dissociation probability $P(E,T)$, can be expressed by $J_{ph} = qG_{max}P(E,T)L$. Thus, the values of $P(E,T)$ at any V_{eff} can be obtained from the ratio of J_{ph}/J_{sat}. It was calculated that $P(E,T)$ values under the short-circuit condition increased from 94.6% for the device without the inserted-PCBM layer to 96.7% for the device with the 15 nm inserted-PCBM layer, which demonstrates that the inserted-PCBM layer is beneficial for the dissociation of excitons into free charge carriers. Due to the enhanced exciton generation rate and the exciton dissociation probability, the photocurrent density was increased for the device with the 15 nm inserted-PCBM layer.

Fig. 3 shows the impedance response (measured in the dark) of the devices with different thicknesses of the inserted-PCBM layer (0 nm to 20 nm) in a frequency range of 0.1 Hz to 1 MHz with an oscillation amplitude of 10 mV. It is noticeable that at high frequencies, the spectra of the five devices almost overlap. As the frequency decreases, the five curves gradually separate from each other. It can be observed that the diameters of the five semicircles are different from each other. In impedance

Table 1 Parameters of the five investigated devices

Thickness of inserted PCBM (nm)	V_{OC} (V)	J_{SC} (mA cm^{-2})	FF (%)	PCE (%)	Average PCE (10 devices)	R_s (Ω cm^2)	R_{sh} (kΩ cm^2)
0	0.616	9.17	61.9	3.57	3.55	11.58	1.10
5	0.617	9.37	65.1	3.76	3.72	8.39	1.61
10	0.615	10.05	67.7	4.19	4.04	7.00	2.04
15	0.615	10.06	68.5	4.24	4.16	6.60	2.28
20	0.615	9.69	65.8	3.92	3.91	8.24	1.95

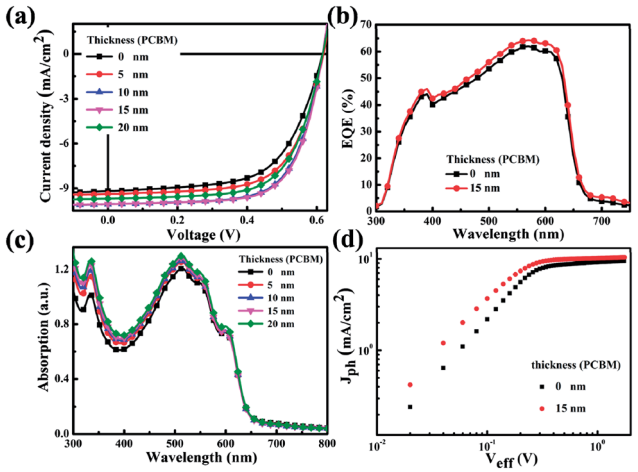

Fig. 2 (a) *J*–*V* curves of the investigated devices. (b) EQE spectra of the device without the inserted-PCBM layer and the device with the 15 nm inserted-PCBM layer. (c) The absorption spectra of the devices. (d) The photocurrent density *versus* effective voltage characteristics of the device without the inserted-PCBM layer and the device with the 15 nm inserted-PCBM layer.

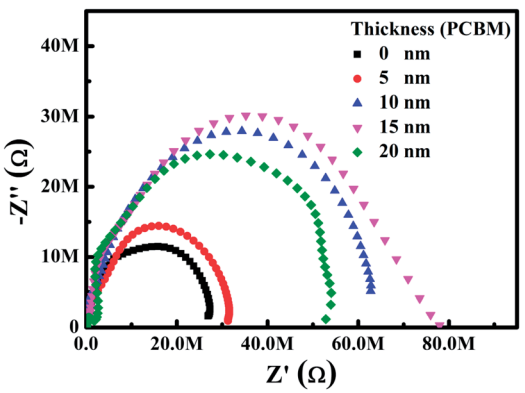

Fig. 3 The impedance spectra of the five devices (measured in the dark).

spectroscopy, the diameter of the semicircle basically represents the shunt resistance of the device under its test conditions.[30–32] It is seen that the device with the 15 nm inserted-PCBM layer has the largest shunt resistance among all of these devices, which is consistent with its best photovoltaic performance. Detailed investigation also shows that a higher shunt resistance (extracted from Fig. 3) corresponds to better device performance (shown in Table 1): a higher FF and PCE.

To evaluate the distribution of P3HT and PCBM on the surface (about 0–10 nm) of the active layers, X-ray photoelectron spectroscopy (XPS) was used to probe the atom distribution of oxygen, sulphur and carbon for the film without the inserted-PCBM layer and the film with a 15 nm inserted-PCBM layer. Because the oxygen atom only exists in PCBM and the sulphur atom only exists in P3HT, the distribution of the atoms can be used to speculate semi-quantitatively how the materials of P3HT and PCBM are distributed in the surface of the active layers. Fig. 4(a) presents the S, O and C spectra, which exhibit strong S2p, S2s and C1s peaks at around 164 eV, 230 eV and 285 eV, respectively, and then a weak O1s peak at around 533 eV.[33–35] It can be clearly observed from Fig. 4(b) and (c) (both are enlarged spectra) that the S and O peaks from the film without the inserted-PCBM layer and the film with the 15 nm inserted-PCBM layer match perfectly with each other. Additionally, another important factor is the number ratio of O, S and C atoms to their sum. The XPS results reveal that the atom percentages of O, S and C are 1.05%, 7.6% and 91.35% respectively for the film without the inserted-PCBM layer, while for the film with the 15 nm inserted-PCBM layer, the atom percentages of O, S and C are 1.39%, 7.12% and 91.49%, respectively. The existence of P3HT (indicated by the existence of S atoms) shows that the inserted-PCBM layer will diffuse into

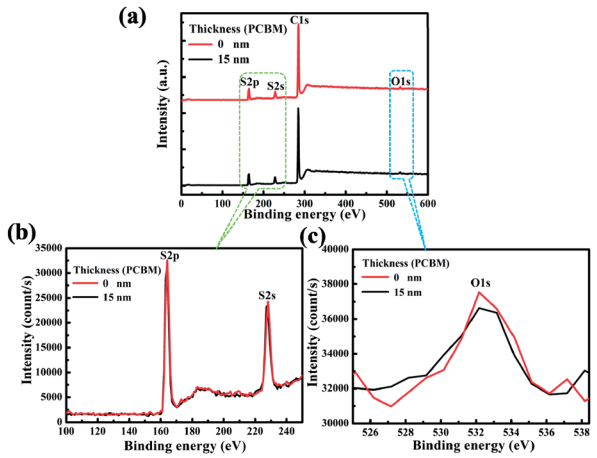

Fig. 4 (a) The S2p, S2s, C1s and O1s peaks from XPS of the active layer surfaces without and with the 15 nm inserted PCBM layer. (b) Magnified S2p and S2s peaks. (c) Magnified O1s peak.

the underlying blend layer of P3HT:PCBM during the post-annealing process (an annealing process before depositing the Ca/Al cathode). Nevertheless, the initial covering layer of the inserted-PCBM results in more PCBM on the surface region after annealing in comparison to the film without an inserted-PCBM layer (indicated by the higher atom ratio of O: 1.39% *vs.* 1.05%). The increase of PCBM on the surface is beneficial to form a good contact between the active layer and the cathode electrode, suppressing carrier recombination and facilitating carrier extraction, and as a result the device performance is enhanced. Fig. S1† in the ESI shows Atomic Force Microscopy (AFM) images of the P3HT:PCBM films without the PCBM buffer layer and with the 15 nm PCBM buffer layer. It was revealed that the root mean square (RMS) roughness of these two films was 16.1 nm and 9.9 nm, respectively. The smoother surface induced by the inserted-PCBM layer could also help form good contact between the active layer and the cathode electrode, and hence enhance the device performance.

We also tried C_{60} and indene-C_{60} bisadduct (ICBA) as inserted functional layers, however they did not work well. The device structures with inserted C_{60} and ICBA layers are presented in Fig. 5(a) and (b), respectively. Fig. 5(c) shows the *J–V* curves of the C_{60}-based devices (the inserted-C_{60} layer thickness varies from 0 to 15 nm), and the *J–V* curves of the ICBA-based devices are presented in Fig. 5(d) (the inserted-ICBA layer thickness is from 0 to 15 nm). It is noticeable that for both of the C_{60} and ICBA based devices, their performances are worse than that of the standard P3HT:PCBM and P3HT:ICBA devices. We are not clear why they do not work well but here we offer a tentative explanation. For C_{60} based devices, C_{60} could be an impurity in the active layer of the P3HT:PCBM blend because the lowest unoccupied molecular orbital (LUMO) of C_{60} is lower than that of PCBM, hence certain electrons generated in the P3HT:PCBM blend will flow from PCBM to C_{60}. Some will be directly collected by the cathode electrode in areas where C_{60} is directly in contact with the cathode and some electrons will be trapped in the C_{60} if the C_{60} is isolated from the cathode electrode by either PCBM or P3HT. Therefore, the inserted C_{60} layer plays a role of deteriorating the device performance. For the ICBA-based devices, it noticeable that the device performance is greatly reduced even with an ultrathin 5 nm ICBA layer. As reported in previous works, there are many isomers for ICBA.[36,37] Hence, the evaporated ICBA could contain various isomers, which could seriously harm the quality of the interface between the active layer and the cathode electrode, and hence worsen the overall device performance.

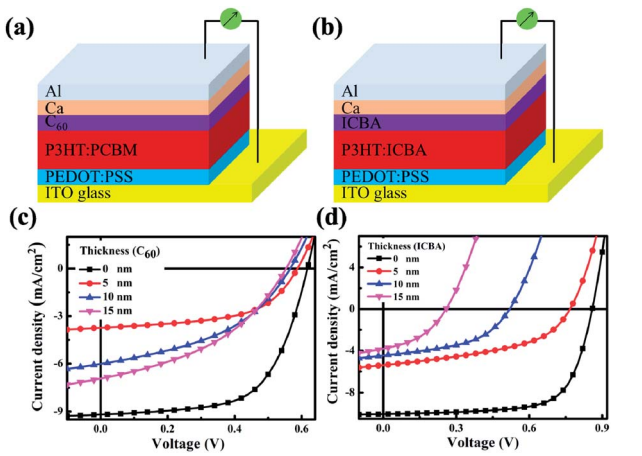

Fig. 5 Device structure with (a) the C_{60} inserted layer and (b) the ICBA inserted layer. *J–V* curves of (c) C_{60}-based and (d) ICBA-based devices.

Conclusions

In summary, P3HT:PCBM solar cells with inserted-PCBM layers (between the P3HT:PCBM blend and the cathode electrode) were fabricated and investigated. The inserted-PCBM layer can improve the device performance in a wide thickness range of 0 to 20 nm. The maximum PCE of 4.24% was achieved for the device with a 15 nm inserted PCBM layer, which is much higher than that of the traditional standard device without an inserted-PCBM layer (3.57%). Such enhancement is mainly attributed to the improved J_{SC} and FF. It was found that the inserted-PCBM layer can enhance the overall light absorption of the active layer, which leads to an increase in J_{SC}. The inserted-PCBM also increases the amount of PCBM on the surface of the active layer, on which the cathode electrode is deposited. The increase in PCBM at the active layer/cathode interface can decrease surface carrier recombination and help carrier extraction. Due to the advantages that the inserted-PCBM layer brings, the device performance was improved. We also tried to use C_{60} and ICBA as inserted layers for P3HT:PCBM and P3HT:ICBA based solar cells, and found that the two do not work well and possible reasons were proposed.

Experimental

Device fabrication: all devices were fabricated on indium tin oxide (ITO) patterned glass substrates, which were cleaned by detergent and sonicated in deionized water, acetone, and isopropanol for 10 min, respectively. The ITO substrates were exposed to O_2 plasma for 6 min prior to spin-coating with poly(ethylenedioxythiophene):poly(styrenesulfonic acid) (PEDOT:PSS, Baytron PVP A1 4083) at 3000 rpm for 40 s. Next, the PEDOT:PSS-coated substrates were annealed at 140 °C for 10 min in air, and then taken into a nitrogen-filled glove box. The active blend layer of P3HT (regioregular P3HT (4002-E), Rieke Metals Inc):PCBM (Nano-C) (15 : 12 w/w, in *o*-dichlorobenzene) was spin-coated onto the substrates at 500 rpm for 18 s. Then, the active layers were covered in a glass Petri dish and allowed to dry for about 40 min. After that, all of the blend films were annealed on a hot plate at 110 °C for 10 min in a nitrogen glove box to remove any residual solvents. The PCBM insertion layer, with a thickness which varied from 0 nm to 20 nm, was deposited by thermal evaporation over the P3HT:PCBM blend layer. Subsequently, the P3HT:PCBM layer with the deposited PCBM layer was annealed at 110 °C for 10 min. Finally, a ~25 nm Ca and 80 nm Al electrode was evaporated at a base pressure of 10^{-6} Torr through a shadow mask. The devices with the

inserted layer of C_{60} (Nano-C) or ICBA (Nano-C) were fabricated using the same process.

Device measurements: a Keithley 2400 was used to measure the *J–V* characteristics of these devices under AM 1.5 illumination with an intensity of 100 mW cm^{-2} (450 W Newport 6279 NS solar simulator) in N_2 atmosphere. The external quantum efficiency (EQE) spectrum was collected using a Oriel IQE-200™. A Surface Profilometer (Tencor, ALFA-Step 500) was used to estimate the thicknesses of the active layers. The impedance spectroscopy (IS) measurement was performed using a Zahner Zennium electrochemical workstation. X-ray photoelectron spectroscopy (XPS) (using monochromatized Al Kα X-ray photons, *i.e.* $h\nu = 1486.6$ eV, discharge lamp) was applied to measure semi-quantitatively the proportion of oxygen and sulphur atoms for the analysis of the surface distribution of P3HT and PCBM in the active layer.

Acknowledgements

This work was mostly supported by the National Basic Research Program of China (Grant no. 2012CB934200, 2014CB643503), National Natural Science Foundation of China (Contract nos 50990064, 61076009, 61204002), the National Natural Science Foundation of China (Grant nos 61072014 and 21021091), 973 Program (Grant no. 2011CB932304 and 2014CB643606) and the Chinese Academy of Sciences.

Notes and references

1 G. Yu, J. Gao, J. Hummelen, F. Wudl and A. Heeger, *Science*, 1995, **270**, 1789.
2 Y. F. Li, *Acc. Chem. Res.*, 2012, **45**, 723.
3 B. C. Thompson and J. M. Frechet, *Angew. Chem., Int. Ed.*, 2008, **47**, 58.
4 G. Li, R. Zhu and Y. Yang, *Nat. Photonics*, 2012, **6**, 153.
5 Z. He, C. Zhong, S. Su, M. Xu, H. Wu and Y. Cao, *Nat. Photonics*, 2012, **6**, 593.
6 C. E. Small, S. Chen, J. Subbiah, C. M. Amb, S.-W. Tsang, T.-H. Lai, J. R. Reynolds and F. So, *Nat. Photonics*, 2011, **6**, 115.
7 X. Li, W. C. Choy, L. Huo, F. Xie, W. E. Sha, B. Ding, X. Guo, Y. Li, J. Hou, J. You and Y. Yang, *Adv. Mater.*, 2012, **24**, 3046.
8 T. Yang, M. Wang, C. Duan, X. Hu, L. Huang, J. Peng, F. Huang and X. Gong, *Energy Environ. Sci.*, 2012, **5**, 8208.
9 Y. Zhou, C. Fuentes-Hernandez, J. W. Shim, T. M. Khan and B. Kippelen, *Energy Environ. Sci.*, 2012, **5**, 9827.
10 L. Lu, Z. Luo, T. Xu and L. Yu, *Nano Lett.*, 2013, **13**, 59.
11 J. Burschka, N. Pellet, S. J. Moon, R. Humphry-Baker, P. Gao, M. K. Nazeeruddin and M. Gratzel, *Nature*, 2013, **499**, 316.
12 M. Liu, M. B. Johnston and H. J. Snaith, *Nature*, 2013, **501**, 395.
13 Y. Zhu, T. Song, F. Zhang, S.-T. Lee and B. Sun, *Appl. Phys. Lett.*, 2013, **102**, 113504.
14 J. Oh, H.-C. Yuan and H. M. Branz, *Nat. Nanotechnol.*, 2012, **7**, 743.
15 F. Zhang, X. Han, S.-t. Leeand and B. Sun, *J. Mater. Chem.*, 2012, **22**, 5362.
16 L.-M. Chen, Z. Hong, G. Li and Y. Yang, *Adv. Mater.*, 2009, **21**, 1434.
17 W. Ma, C. Yang, X. Gong, K. Lee and A. J. Heeger, *Adv. Funct. Mater.*, 2005, **15**, 1617.
18 G. Li, V. Shrotriya, J. Huang, Y. Yao, T. Moriarty, K. Emery and Y. Yang, *Nat. Mater.*, 2005, **4**, 864.
19 M. S. Ryu, H. J. Cha and J. Jang, *Curr Appl Phys*, 2010, **10**, S206.
20 K. Kim, *Appl. Phys. Lett.*, 2007, **90**, 163511.
21 B. Tremolet de Villers, C. J. Tassone, S. H. Tolbert and B. J. Schwartz, *J. Phys. Chem. C*, 2009, **113**, 18978.
22 Z. Liu and E.-C. Lee, *J. Appl. Phys.*, 2012, **111**, 023104.
23 B. Qi and J. Wang, *Phys. Chem. Chem. Phys.*, 2013, **15**, 8972.
24 J. D. Servaites, S. Yeganeh, T. J. Marks and M. A. Ratner, *Adv. Funct. Mater.*, 2010, **20**, 97.
25 M. S. Kim, B. G. Kim and J. Kim, *ACS Appl. Mater. Interfaces*, 2009, **1**, 1264.
26 J. R. Tumbleston, D.-H. Ko, E. T. Samulski and R. Lopez, *J. Appl. Phys.*, 2010, **108**, 084514.
27 V. Mihailetchi, L. Koster, J. Hummelen and P. Blom, *Phys. Rev. Lett.*, 2004, **93**, 216601.
28 V. D. Mihailetchi, H. Xie, B. de Boer, L. J. A. Koster and P. W. M. Blom, *Adv. Funct. Mater.*, 2006, **16**, 699.
29 J.-L. Wu, F.-C. Chen, Y.-S. Hsiao, F.-C. Chien, P. Chen, C.-H. Kuo, M. H. Huang and C.-S. Hsu, *ACS Nano*, 2011, **5**, 959.
30 B. J. Leever, C. A. Bailey, T. J. Marks, M. C. Hersam and M. F. Durstock, *Adv. Energy Mater.*, 2012, **2**, 120.
31 G. Perrier, R. de Bettignies, S. Berson, N. Lemaître and S. Guillerez, *Sol. Energy Mater. Sol. Cells*, 2012, **101**, 210.
32 G. Garcia-Belmonte, A. Munar, E. M. Barea, J. Bisquert, I. Ugarte and R. Pacios, *Org. Electron*, 2008, **9**, 847.
33 X. Gu, W. Cui, H. Li, Z. Wu, Z. Zeng, S.-T. Lee, H. Zhang and B. Sun, *Adv. Energy Mater.*, 2013, **3**, 1262.
34 Z. Tan, W. Zhang, Z. Zhang, D. Qian, Y. Huang, J. Hou and Y. Li, *Adv. Mater.*, 2012, **24**, 1476.
35 J.-M. Yun, Y.-J. Noh, J.-S. Yeo, Y.-J. Go, S.-I. Na, H.-G. Jeong, J. Kim, S. Lee, S.-S. Kim, H. Y. Koo, T.-W. Kim and D.-Y. Kim, *J. Mater. Chem. C*, 2013, **1**, 3777.
36 C.-H. Cho, H. J. Kim, H. Kang, T. J. Shin and B. J. Kim, *J. Mater. Chem.*, 2012, **22**, 14236.
37 H.-Y. C. Youjun He, J. Hou and Y. Li, *J. Am. Chem. Soc.*, 2010, **132**, 1377.